SINTEF
PROCEEDINGS
1

Selected papers from 10th International Conference on Computational Fluid Dynamics in the Oil & Gas, Metallurgical and Process Industries

Progress in Applied CFD

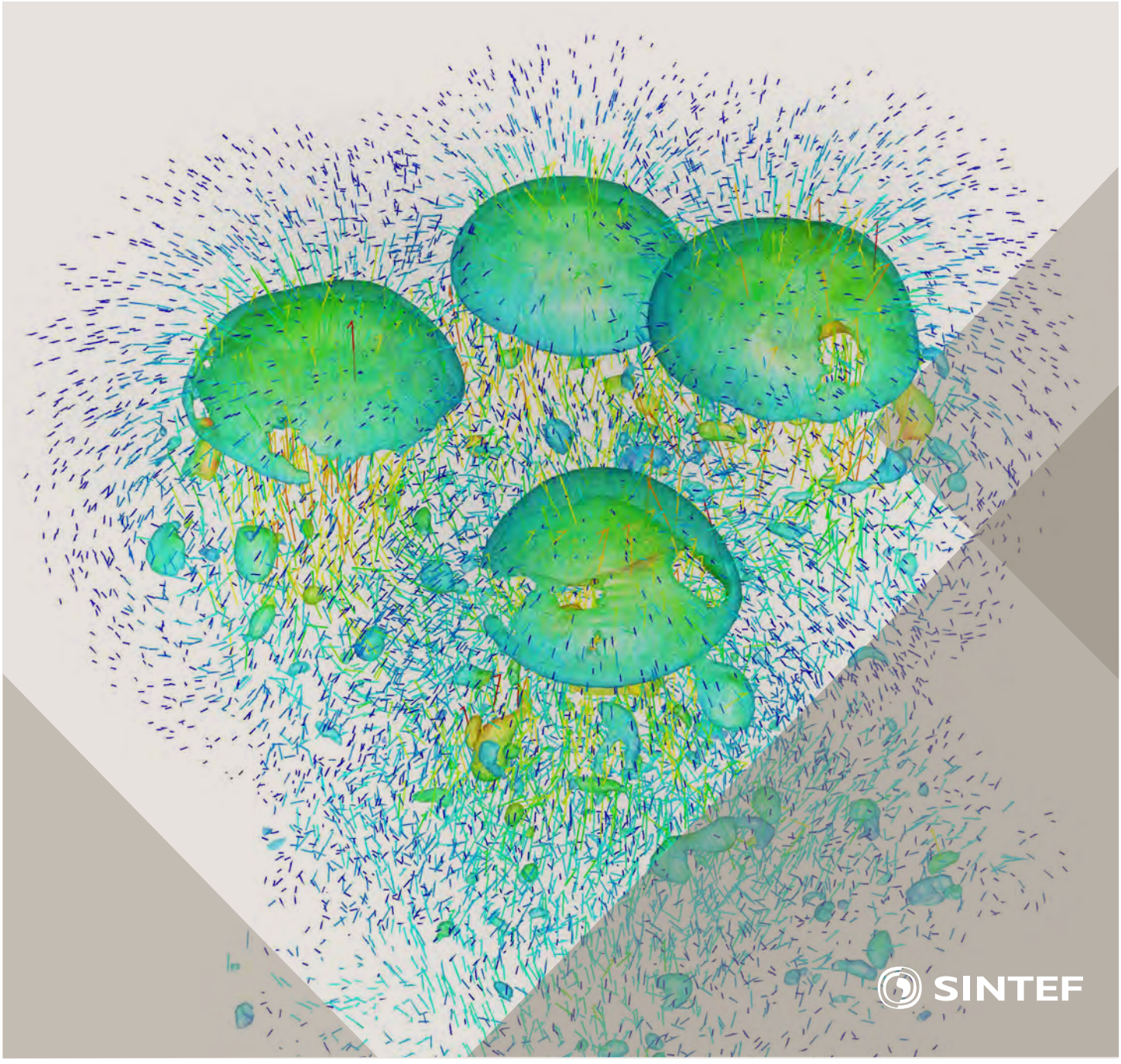

SINTEF Proceedings

Editors:
Jan Erik Olsen and Stein Tore Johansen

Progress in Applied CFD

Selected papers from 10th International Conference on Computational Fluid Dynamics in the Oil & Gas, Metallurgical and Process Industries

SINTEF Academic Press

SINTEF Proceedings no 1
Editors: Jan Erik Olsen and Stein Tore Johansen
Progress in Applied CFD
Selected papers from 10th International Conference on Computational Fluid Dynamics in the Oil & Gas, Metallurgical and Process Industries

Key words:
CFD, Flow, Modelling

Cover, illustration: Rising bubbles by Schalk Cloete

ISSN 2387-4287 (printed)
ISSN 2387-4295 (online)
ISBN 978-82-536-1432-8 (printed)
ISBN 978-82-536-1433-5 (pdf)

60 copies printed by AIT AS e-dit
Content: 100 g munken polar
Cover: 240 g trucard

© Copyright SINTEF Academic Press 2015
The material in this publication is covered by the provisions of the Norwegian Copyright Act. Without any special agreement with SINTEF Academic Press, any copying and making available of the material is only allowed to the extent that this is permitted by law or allowed through an agreement with Kopinor, the Reproduction Rights Organisation for Norway. Any use contrary to legislation or an agreement may lead to a liability for damages and confiscation, and may be punished by fines or imprisonment

SINTEF Academic Press
Address: Forskningsveien 3 B
PO Box 124 Blindern
N-0314 OSLO
Tel: +47 22 96 55 55
Fax: +47 22 96 55 08

www.sintef.no/byggforsk
www.sintefbok.no

SINTEF Proceedings
SINTEF Proceedings is a serial publication for peer-reviewed conference proceedings on a variety of scientific topics.
The processes of peer-reviewing of papers published in SINTEF Proceedings are administered by the conference organizers and proceedings editors. Detailed procedures will vary according to custom and practice in each scientific community.

PREFACE

This book contains selected papers from the 10th International Conference on Computational Fluid Dynamics in the Oil & Gas, Metallurgical and Process Industries. The conference was hosted by SINTEF in Trondheim in June 2014 and is also known as CFD2014 for short. The conference series was initiated by CSIRO and Phil Schwarz in 1997. So far the conference has been alternating between CSIRO in Melbourne and SINTEF in Trondheim. The conferences focus on the application of CFD in the oil and gas industries, metal production, mineral processing, power generation, chemicals and other process industries. The papers in the conference proceedings and this book demonstrate the current progress in applied CFD.

The conference papers undergo a review process involving two experts. Only papers accepted by the reviewers are presented in the conference proceedings. More than 100 papers were presented at the conference. Of these papers, 27 were chosen for this book and reviewed once more before being approved. These are well received papers fitting the scope of the book which has a slightly more focused scope than the conference. As many other good papers were presented at the conference, the interested reader is also encouraged to study the proceedings of the conference.

The organizing committee would like to thank everyone who has helped with paper review, those who promoted the conference and all authors who have submitted scientific contributions. We are also grateful for the support from the conference sponsors: FACE (the multiphase flow assurance centre), Total, ANSYS, CD-Adapco, Ascomp, Statoil and Elkem.

Stein Tore Johansen & Jan Erik Olsen

Organizing committee:

Conference chairman: Prof. Stein Tore Johansen
Conference coordinator: Dr. Jan Erik Olsen
Dr. Kristian Etienne Einarsrud
Dr. Shahriar Amini
Dr. Ernst Meese
Dr. Paal Skjetne
Dr. Martin Larsson
Dr. Peter Witt, CSIRO

Scientific committee:

J.A.M.Kuipers, TU Eindhoven
Olivier Simonin, IMFT/INP Toulouse
Akio Tomiyama, Kobe University
Sanjoy Banerjee, City College of New York
Phil Schwarz, CSIRO
Harald Laux, Osram
Josip Zoric, SINTEF
Jos Derksen, University of Aberdeen
Dieter Bothe, TU Darmstadt
Dmitry Eskin, Schlumberger
Djamel Lakehal, ASCOMP
Pär Jonsson, KTH
Ruben Shulkes, Statoil
Chris Thompson, Cranfield University
Jinghai Li, Chinese Academy of Science
Stefan Pirker, Johannes Kepler Univ.
Bernhard Müller, NTNU
Stein Tore Johansen, SINTEF
Markus Braun, ANSYS

CONTENTS

A SIX CHEMICAL SPECIES CFD MODEL OF ALUMINA REDUCTION IN A HALL-HÉROULT CELL

Peter J. WITT[1*], Yuqing FENG[1], Graeme A. SNOOK[1], Ingo EICK[2] and Mark COOKSEY[1]
[1] CSIRO Mineral Resources Flagship, Melbourne 3169, AUSTRALIA
[2] Hydro Aluminium Deutschland GmbH, Neuss, GERMANY

* E-mail: peter.witt@csiro.au

ABSTRACT

The industrial process for producing primary aluminium metal is the reduction of powdered alumina in a Hall-Héroult reduction cell. These cells operate at temperatures above 940 °C with a highly corrosive electrolyte making physical measurement of the process difficult or nearly impossible. Computational models of the electro-magnetic fields and heat transfer are widely used in industry to design cells. Only recently (Feng et al., 2010b, Witt et al., 2012) have detailed computational models of the molten liquid-gas bath become available. Alumina distribution within the cells is important for cell efficiency and preventing anode effects. Using the bath flow information and an assumption of uniform reduction, a single scalar transport equation has been used to track the time variation of alumina within cells (Feng et al., 2011).

In this work the previous single species model is extended to include six chemical species and four chemical reactions. The reaction pathway developed for the model is that solid alumina particles are fed to the bath surface, where they mix and submerge into the liquid bath, and then undergo dissolution from solid particles to the liquid species $Na_2Al_2O_2F_4$. Within the bath $Na_2Al_2O_2F_4$ converts to $Na_2Al_2OF_6$, which is involved in an oxidation reaction with carbon to produce carbon dioxide and AlF_3 at the anode surface. At the metal pad a cathodic reaction occurs with AlF_3 converting to aluminium metal. Species solubility rates are based on the work of Solheim et al. (1995).

A CFD model of a single anode in a bubbly cryolite bath was built based on a corner anode from an industrial cell. Steady state bath flows were calculated and used to transport the six chemical species in the new bath chemistry model. Results were obtained for 20,000 seconds of real time for species distributions in the anode to cathode distance (ACD), change in mass of species in the bath with time, rates for the four reactions at locations in the bath and change in the species mass fraction with time at various locations during a feeding cycle.

Keywords: CFD, Process metallurgy, Alumina reduction chemistry, Hall-Héroult aluminium cell, Multiphase chemistry.

NOMENCLATURE

Symbols

A_{Anode} Anode surface area, [m^2]
$A_{Cathode}$ Cathode surface area, [m^2]
F Faradays constant = 96 485 [A s mol^{-1}]
J_{Anode} Current density at anode, [A m^{-2}]
$J_{Cathode}$ Current density at cathode, [A m^{-2}]
k_1 Reaction rate equation (1), [mol s^{-1}]
k_2 Reaction rate equation (2), [mol s^{-1}]
k_3 Reaction rate equation (3), [mol s^{-1}]
k_4 Reaction rate equation (4), [mol s^{-1}]
r Cryolite ratio (molar ratio of NaF and AlF_3)
x_1 Molar fraction of $Na_2Al_2OF_6$
x_2 Molar fraction of $Na_2Al_2O_2F_4$
Y_i Mass fraction for species *i*

Sub/superscripts

a Anode
c Cathode
i Index *i.*

INTRODUCTION

The Hall-Héroult process is the dominant industrial scale technology for reducing alumina powder to primary aluminium metal. Reduction cell performance is dependent on a mix of complex physical processes that occur in the cell and includes electrochemical, electro-magnetic, heat transfer and hydrodynamic processes.

Alumina particles are periodically feed on to the top of this molten cryolite bath; these particles then dissolve into the bath. Electrical current is supplied to the cell through anodes that are partially immersed into the top of the bath. Through an electrochemical reaction this electrical current reduces alumina in the presence of carbon anode to aluminium metal and carbon dioxide. Evolved carbon dioxide gas forms bubbles under the anodes where buoyancy forces cause these bubbles to

travel along the anode's base, before they rise to the surface beside the anode. A strong internal flow of liquid bath is established by the bubble motion and this acts to transport alumina and heat through the bath. Aluminium metal, reduced by the reaction, forms a layer of molten metal in the bottom of the cell.

Aluminium reduction cells operate in a harsh environment as the bath is molten cryolite, known to dissolve most engineering materials, and at a temperature of approximately 940°C. Electrical currents in the range of 100 to 450 kA are typical in reduction cells. Such currents induce strong magnetic fields, which act on conducting liquid metal and the molten bath, inducing secondary flows by Lorentz forces. These conditions along with restricted access make measurements on operating cells very difficult and greatly limit the amount of information that can be obtained.

To develop new cells and to improve the economic and environmental performance of existing cells, new tools are needed. Moxnes et al. (2009) described how optimised alumina feeding through experimentation can improve performance. However, experimentation is very costly and time consuming. Mathematical models can provide a tool to understand and explore how changes to cell geometry and operation affect performance (Gusberti et al. 2012). Thus validated mathematical models can provide a more efficient means of achieving improved cell performance than through experimentation.

The above description of the alumina reduction process is vastly simplified but has been successfully used previously to develop a computational fluid dynamics (CFD) model of alumina distribution in these cells. Feng *et al.* (2010a) and Feng *et al.* (2011) tracked an alumina species using a predicted bath flow field and assumed that uniform reduction occurred throughout the anode to cathode distance (ACD) under the anodes. Alumina distribution within the cell and feeding policies were able to be investigated; such an investigation was reported by Feng et al. (2010a).

In practice the bath consists of a number of ionic species that undergo a series of complex reactions. Work such as those by Gagnon *et al.* (2011), Kvande (1986) Mandin *et al.* (2009) and Solheim (2012) among others have proposed reaction models and bath species. All have assumed species transport by diffusion or simple hydrodynamic models.

In this work we extend the earlier alumina distribution model of Feng *et al.* (2011) to include six chemical species so as to more accurately represent the underlying electro-chemistry occurring in Hall-Héroult cells.

MODEL DESCRIPTION

The CFD modelling approach used in this work is to solve a steady-state model for the bath and bubble flow within a cell. Then by holding the bath flow fixed a transient model of species transport, alumina feeding and reactions is used to predict the time varying species concentration in the cell.

Details of the CFD model physics, approach and implementation in ANSYS/Fluent (ANSYS, 2013) have been previously documented in previous works Feng *et al.* (2010a, 2010b, 2011) and Witt *et al.* (2012). For brevity only an overview of the bath flow model is presented here.

The bath flow model describes the steady state flow of both gas and liquid phases based on a time averaged method. Key features of the bath flow model are:

- Gas and liquid flow are modelled using the Eulerian-Eulerian or two-fluid approach,
- Small-scale structures such as bubbles and turbulent structures are averaged in time and space,
- Drag from the bubbles is modelled using the Ishii and Zuber (1979) drag law,
- Turbulent effects are modelled using the k-ε turbulence model with modifications for multiphase flow to include, turbulent dispersion Lopez de Bertodano (1991), bubble induced turbulence (Smith, 1998 and Olmos *et al.*, 2003) and enhanced turbulent viscosity,
- Electro-magnetic effects are included through the Lorentz force, which is calculated from magnetic and electric fields for a typical pot line.

The alumina distribution model describes the transient distribution of alumina and other chemical species within the liquid bath. Transport of alumina and other chemical species is based on the steady state bath flow model.

The key stages in reduction of alumina to aluminium metal are:

- **Feeding** of alumina to the bath surface, this can occur at various times and at a number of locations,
- **Initial breakup, mixing** and submersion of particles from the surface into the liquid bath, assumed to occur over 10 seconds, this is used to set a boundary condition for the alumina such that the mass from a feed event is averaged over a 10 second period,
- **Dissolution** of alumina particles into the bath through the reaction:

$$Al_2O_{3(sol)} + 3\,NaF + AlF_3 \overset{k1}{\Rightarrow} \frac{3}{2}\,Na_2Al_2O_2F_4 \qquad (1)$$

- **Equilibrium** bath reaction:

$$Na_2Al_2O_2F_4 + 2\,NaF + 2\,AlF_3 \overset{k2}{\Leftrightarrow} 2\,Na_2Al_2OF_6 \qquad (2)$$

- **Anode** boundary layer reaction:

$$2\,Na_2Al_2OF_6 + C \overset{k3}{\Rightarrow} 4e^- + 4\,AlF_3 + 4\,Na^+ + CO_2 \qquad (3)$$

- **Cathode** or metal pad boundary layer reaction:

$$AlF_3 + 3\,Na^+ + 3e^- \overset{k4}{\Rightarrow} Al + 3\,NaF \qquad (4)$$

Reactions rates are required for equations (1) to (4).

The rate for alumina dissolution into the bath is based on the work of Frolov *et al.* (2007) who observed

alumina dissolution in both an industrial bath and a modified bath with fast dissolution properties. By fitting two straight lines to their data for the industrial cell, as shown in Figure 1, the following rate equation can be obtained:

$$k_1 = \max(0, 0.35 - \frac{0.35}{0.03} Y_{Al2O3dis}, 0.164 - \frac{0.164}{0.07} Y_{Al2O3dis}) \quad (5)$$

To limit the reaction in areas of low undissolved alumina the equation is modified to:

$$k_1 = (1.0 - e^{-500 Y_{Al2O3Und}}) \max(0, 0.35 - \frac{0.35}{0.03} Y_{Al2O3dis}, 0.164 - \frac{0.164}{0.07} Y_{Al2O3dis}) \quad (6)$$

Where $Y_{Al2O3dis}$ is the mass fraction of dissolved alumina in the bath and $Y_{Al2O3Und}$ the undissolved alumina in the bath. In this work the dissolved alumina species are $Na_2Al_2O_2F_4$ and $Na_2Al_2OF_6$.

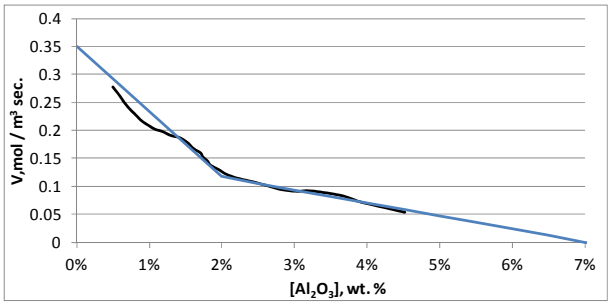

Figure 1: Dissolution rate of alumina in industrial baths at temperature 960 °C from Frolov *et al.* (2007) – black line and the model of equation (5) – blue line.

For equation (2), data from Solheim and Sterten (1999) was used to derive the equilibrium condition that was reported in Solheim (2013) as:

$$\frac{x_1^2}{x_2} = 11.3e^{-2.63r} \quad (7)$$

where x_1 and x_2 are the molar fractions of $Na_2Al_2OF_6$ and $Na_2Al_2O_2F_4$ respectively, and r is the molar ratio (Cryolite Ratio) of NaF and AlF_3. From the equilibrium condition in equation (7), the reaction rate, k_2, needed to bring the two species into equilibrium in that time step is determined.

Reaction rates for the anode and cathode reactions (equations (3) and (4)) are based on the current density such that:

$$k_3 = \frac{J_{Anode} dA_a}{4F} \quad (8)$$

and

$$k_4 = \frac{J_{Cathode} dA_c}{3F} \quad (9)$$

where J_{Anode} is the current density at the anode, $J_{Cathode}$ is the current density at the cathode, F is Faradays constant and dA_a is surface area of the anode and cathode.

Since the current density is not solved in the model, a fixed value at the anode of 0.9 [A cm^{-2}] is used and then, assuming conservation of charge, the cathode current density is $J_{Cathode} = J_{Anode} \frac{A_{anode}}{A_{cathode}}$.

GEOMETRY AND BOUNDARY CONDITIONS

Geometry for the single anode model was based on a Hydro Aluminium HAL300 cell and is shown in Figure 2. The full industrial cell has 30 anodes, to simplify the model for this work a corner anode from the full cell was built, including a typical ledge profile, and meshed using ANSYS/ICEM to give 124,000 hexahedral cells. The anode had two slots; the centreline of the full cell is treated using a symmetry plane while the inter-anode gap is considered to be a vertical wall.

Details of the physics and boundary conditions used are as per the full cell model reported in Witt *et al.* (2012). Gas enters the model through the anode base coloured red in Figure 2. Gas leaves the domain through the free surface coloured green via a degassing boundary condition. Alumina feeding could be varied to different positions in the cell and in this work was to the top of the side channel of the cell through the purple region shown in Figure 2. Each feed was chosen to be 0.15 kg of alumina uniformly added over a 10 second period and was added every 80 seconds.

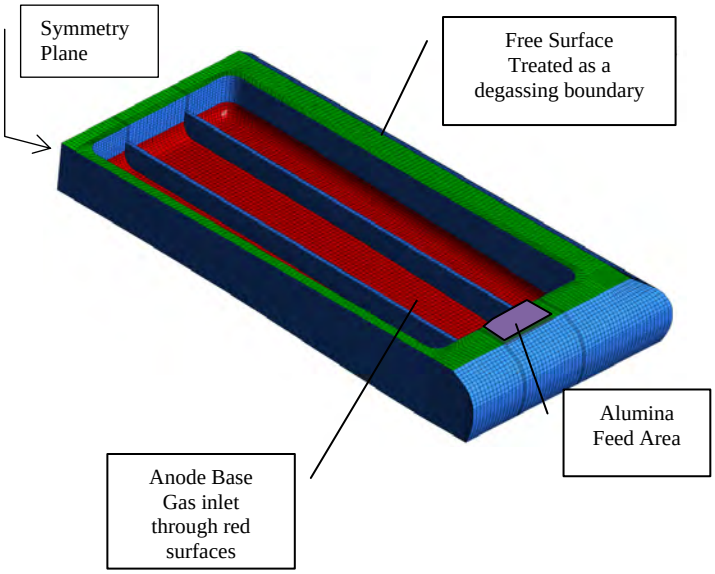

Figure 2: Single Anode Model Geometry.

Initial concentrations for the mass fractions are given in Table 1, which gives a cryolite ratio of 2.2, from which the equilibrium condition for $Na_2Al_2OF_6$ and $Na_2Al_2O_2F_4$ can be determined. The model was run for a time of 20,000 seconds with 1 second time steps.

Table 1: Initial Species mass fraction in the Single Anode Model.

Al_2O_3	$Na_2Al_2O_2F_4$	$Na_2Al_2OF_6$	Na	NaF	AlF_3
0.025[1]	0.044[2]	0.084[2]	0.070[2]	0.420[2]	0.382[2]

[1] Mass fraction of total liquid phase
[2] Mass fractions of dissolved species

RESULTS

For the single anode model the steady state bath flow model was first run to calculate the bath flow field. Results for the bath flow are shown by the streamlines plotted in Figure 3, velocity vectors in the ACD plotted in Figure 4 and the gas volume fraction plotted on two vertical slices near the centre of the anode in Figure 5. These plots show that the model predicts a thin gas layer under the anode that drives a strong bath flow under the anode towards the centre channel. Liquid bath then flows to the end channel, along the end channel and back to the side channel.

Using PIV measurements the bath flow model formulation used in this work was validated for a three anode water model by Feng *et al.* (2010b), thus we expect that the current model should also predict reasonable results. Geometry used by Feng *et al.* (2010b) differs from the current geometry in a number of keys areas: a single anode rather than three anodes, a narrower centre channel, shaped external cell walls due to ledge formation rather than vertical walls, slotted rather than unslotted anodes and an anode slope of nearly 2° upward at the centre channel compared to the flat anodes in the earlier work. These changes prevent direct comparison and have an effect on the flow field. Measurements reported by Feng *et al.* (2010b) show the velocity in the ACD can exceed 0.12 m s^{-1} with a complex flow field. Due to the sloping base of the current anode, which will create stronger and more directional buoyancy forces, flow is directed along the anode length to the centre channel and velocity in the ACD is higher with predicated values up to 0.2 m s^{-1}.

Analysis of streamlines indicates that the travel time for the bath from the side channel under the anode to the centre channel and back along the end channel is approximately 50 seconds.

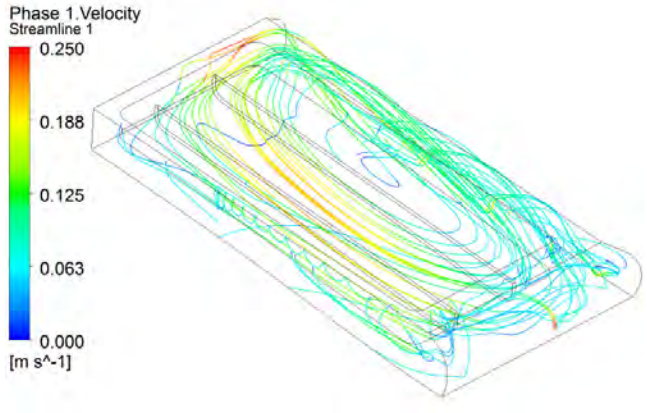

Figure 3: Streamlines showing the bath flow in the Single Anode Model.

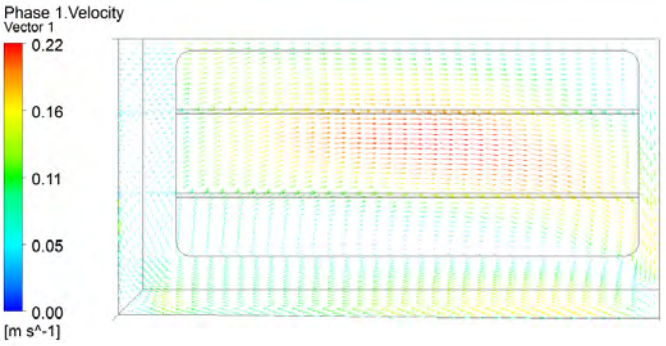

Figure 4: Liquid velocity vectors on a plane through the ACD showing the bath flow in the Single Anode Model.

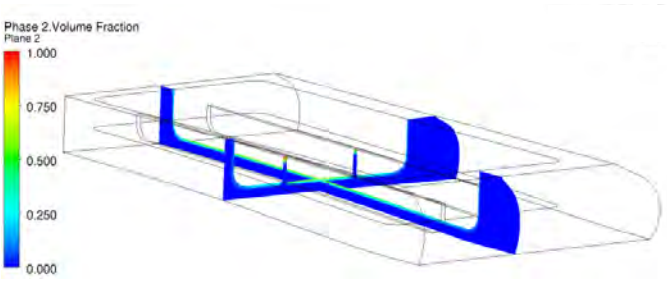

Figure 5: Gas volume fraction on two vertical planes in the Single Anode Model.

Mass fractions for the undissolved and dissolved alumina species considered in the single anode model are plotted on two vertical planes in Figures 6 to 8 after 20,000 seconds (5 hrs 33 minutes). This time instant was selected as it is just before a feed of alumina is about to occur and thus is likely to be close to the point of minimum alumina concentration under the anode. Low alumina concentration in the ACD is one potential cause of anode effects. As alumina is fed to the top of the side channel, undissolved alumina mass fraction is highest in the side channel but lowest in the inter-anode gap and centre channel. The dissolved alumina species in Figures 7 and 8 have a similar concentration distribution to the alumina but note that the plot range is very narrow to highlight the distribution within the cell.

The reaction rate for the dissolution reaction is shown in Figure 9 and indicates that the rate is constant through the cell. The equilibrium reaction rate is plotted in Figure 10 and shows that the reaction proceeds strongly under the anode and reverses in parts of the side and end channels. Figure 11 plots the reaction rate for the anode reaction, and shows the reaction has a slightly lower rate in the centre of the anode due to the gas holdup. The cathode reaction rate is not shown as it is uniform across the metal pad surface.

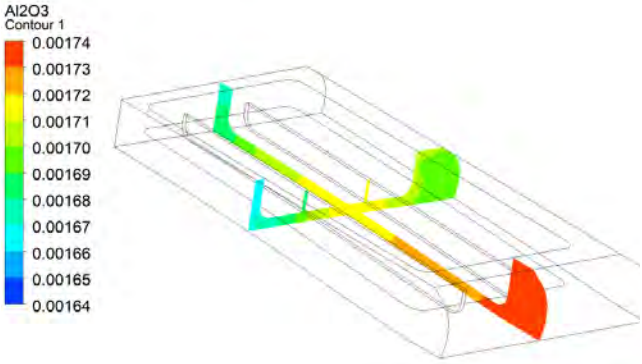

Figure 6: Undissolved alumina mass fraction on two vertical planes in the Single Anode Model at 20,000 [s].

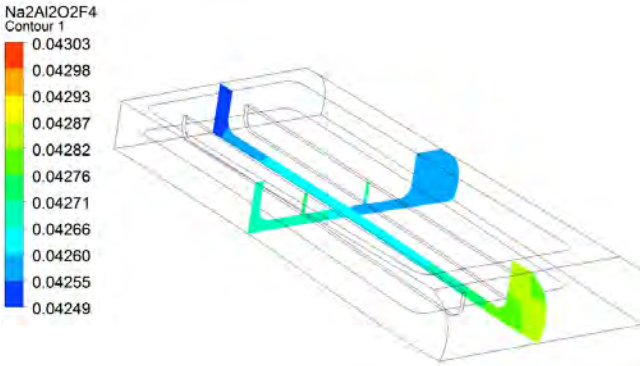

Figure 7: $Na_2Al_2O_2F_4$ mass fraction on two vertical planes in the Single Anode Model at 20,000 [s].

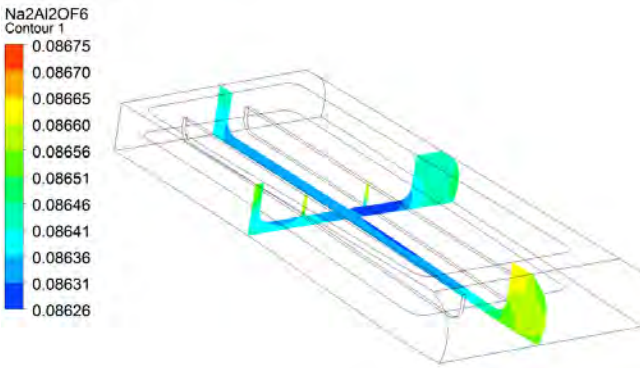

Figure 8: $Na_2Al_2OF_6$ mass fraction on two vertical planes in the Single Anode Model at 20,000 [s].

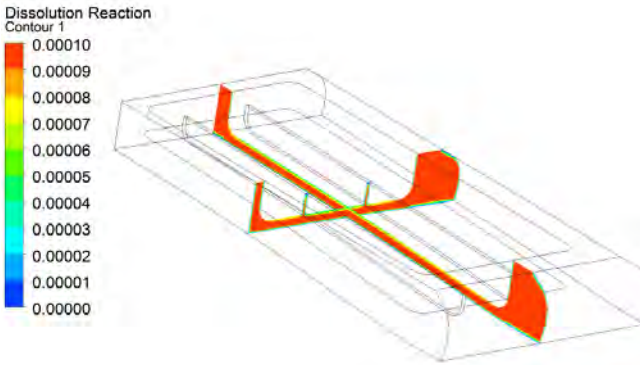

Figure 9: Dissolution reaction rate on two vertical planes in the Single Anode Model at 20,000 [s].

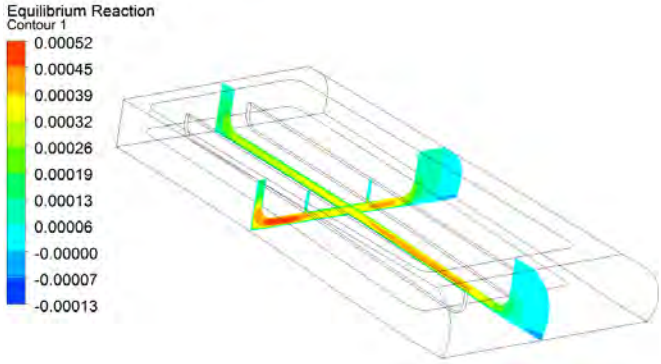

Figure 10: Equilibrium reaction rate on two vertical planes in the Single Anode Model at 20,000 [s].

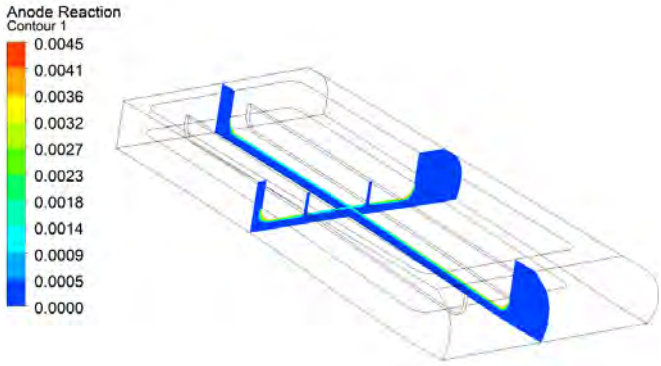

Figure 11: Anode reduction reaction rate on two vertical planes in the Single Anode Model at 20,000 [s].

Figure 12 shows the variation in undissolved alumina on a plane through the centre of the ACD at 20,000 seconds. The magnitude of the variation in species mass fraction is not great but results indicate regions of higher and lower concentrations. Figure 13 plots the equilibrium reaction rate on a plane through the ACD. The equilibrium reaction rate is the fastest under the one-third of the anode near the inter-anode gap and the reaction is predicted to reverse in the side and end channels.

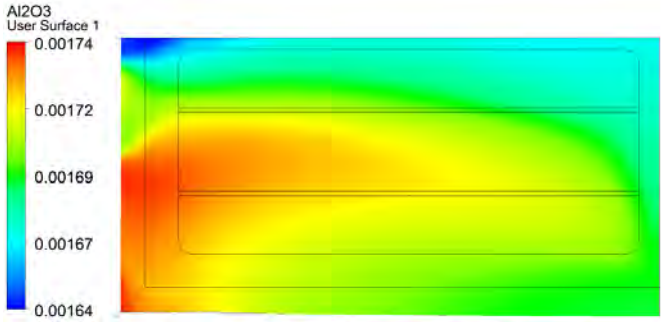

Figure 12: Undissolved alumina mass fraction on a plane through the ACD in the Single Anode Model at 20,000 [s].

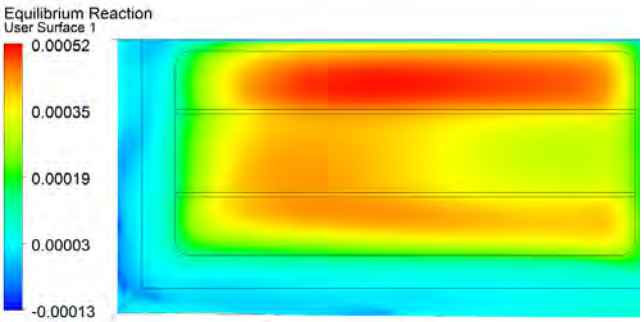

Figure 13: Equilibrium reaction rate on a plane through the ACD in the Single Anode Model at 20,000 [s].

The total mass of the chemical species in the bath and how they change with time is plotted in Figures 14 to 16. In Figure 14 the mass of alumina in the bath varies due to periodic feeding, as shown by the inset; this results in what appears as a wide band for the alumina mass at any time instant. The initial condition for this run was an undissolved alumina mass of 0.984 kg; this reduced rapidly to between 0.7 and 0.8 kg after about 5,000 seconds. After this time the mass is reducing slightly indicating the bath has not completely reached a steady operating condition, but is close to a steady condition. Two other preliminary calculations were run; one with a zero initial undissolved alumina concentration and one with the initial mass set to 4 kg. Both of these showed significant changes in the mass of alumina but would require significantly more than 20,000 seconds before reaching a steady condition. From these preliminary calculations the initial value of 0.984 kg was identified as being close to the steady condition. Mass of the other bath species are plotted in Figures 15 and 16 and show slight changes in their mass with time.

Based on the above results it was concluded that the model was at close to stable operating species concentrations and conditions at 20,000 seconds. To assess the magnitude of the change in bath chemistry between feed additions the results at 20,000 seconds were used to restart the model, from which time it was run for a further 100 seconds. During this short run species mass fractions at nine monitoring points were stored at each time step. The locations of the points are shown in Figure 17. Points 1 to 4 are located on the top of the bath with point 1 being at the feed location. The remaining 5 points are located in the ACD with point 6 being near the centre of the anode and the other four located near the anode edge.

Figure 18 plots the change in undissolved alumina at these locations. The mass fraction at the feeding location, Point 1, initially increases from 0.002 to 0.007 during feeding and the initial 10 second immersion. After feeding it drops rapidly back to the steady state condition, indicating that convective transport rapidly disperses the alumina particles. Points 2 and 8 show nearly a 50% rise in concentration approximately 20 seconds after feeding commences. The streamline in Figure 3 and velocity vectors in Figure 4 show the bath flows from the feed location towards the inter-anode gap and then along the anode to the centre channel, which transports the alumina through the cell and results in the increase in alumina concentration at points 2 and 8.

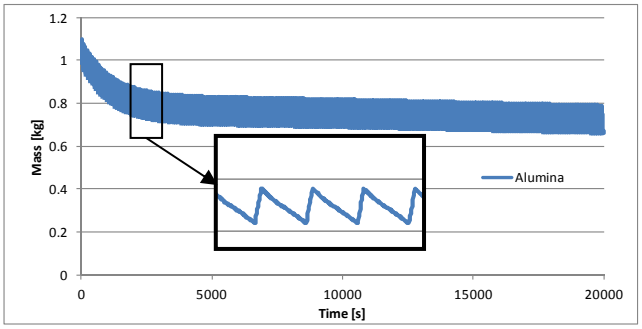

Figure 14: Change in Undissolved Alumina Mass with time for the Single Anode Model.

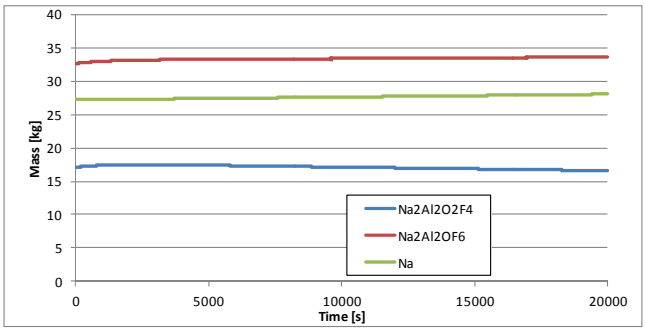

Figure 15: Change in species mass with time for the Single Anode Model.

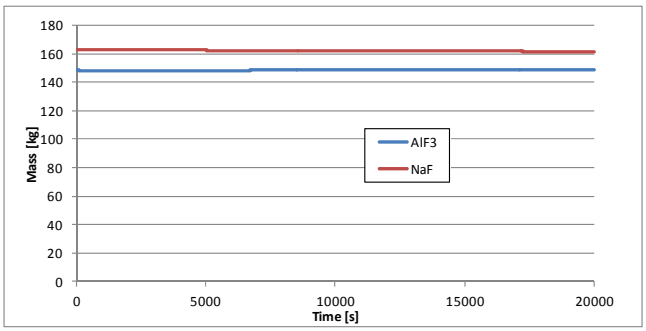

Figure 16: Change in AlF_3 and NaF mass with time for the Single Anode Model.

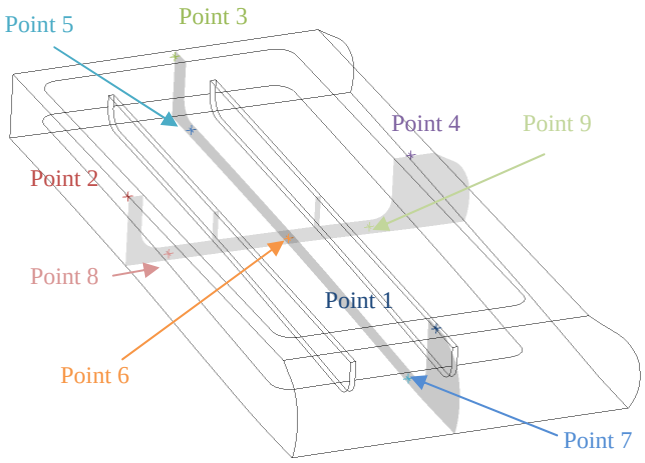

Figure 17: Location of monitoring points in the Single Anode Model.

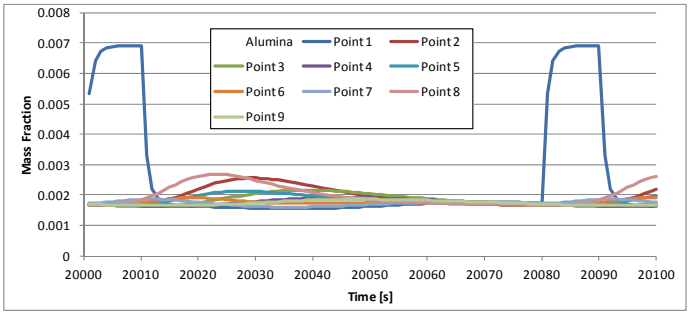

Figure 18: Change in undissolved Alumina mass fraction with time at various locations in the Single Anode Model.

DISCUSSION

The complex reactions, high temperature and harsh chemical environment make direct validation of the single anode model extremely difficult. Based on our past work (Feng *et al.*, 2010a, 2010b and Witt *et al.* 2012) we have a reasonable level of confidence in the bath flow and alumina distribution predictions. Further work using a water model with tracers could be used to improve confidence in the model. Moxnes *et al.* (2009) have used AlF_3 addition to change bath conductivity and measure changes in anode currents. In future work it may be possible to apply this approach to validate the model on a full cell.

For simplicity at the present stage of model development we assume a uniform current distribution across the anode base. This leads to uniform gas generation rate and uniform anode and cathode reaction rates. Clearly this is a simplification as current distribution is non-uniform and a function of gas generated through the anodic reaction. Our plan in future work is to include current distribution in the model and to link the anode and cathode reactions to the local current density. A further complication is our present use of a steady-state bath flow. We propose to iterate between the bath flow and transient chemical reaction models to couple the effects of anode reaction, gas generation, bubble flow and species distribution to overcome limitations in the present approach.

CONCLUSION

We have proposed a new alumina reduction model for the Hall-Héroult process that consists of six chemical species and four reactions. The reaction pathway developed for the model is that solid alumina particles are feed to the bath surface; they take a short time to mix and submerge into the liquid bath, where they undergo dissolution from solid particles to the liquid species $Na_2Al_2O_2F_4$. Within the bath a reaction reduces $Na_2Al_2O_2F_4$ to $Na_2Al_2OF_6$, which is further reduced to carbon dioxide and AlF_3 at the anode surface. At the metal pad a cathodic reaction reacts AlF_3 to form aluminium metal.

A previously published CFD model is used to transport chemical species within the bath based on bubble and MHD driven flow. Reaction for the new bath chemistry model were included in a CFD model and tested on the geometry for a single anode that was run for 20,000 seconds of real time.

Key findings from the model are:

- Preliminary calculations show that if the initial undissolved alumina mass fraction is significantly different from the steady operating state then real times of over 20,000 seconds maybe be required to reach steady conditions.
- Alumina was fed to the top of the side channel and because of this the highest concentration of undissolved alumina was found in the side channel. This location was also where the undissolved alumina mass fraction increased from 0.002 to 0.007 during feeding.
- At a location near the inter-anode gap and midway along the anode the undissolved alumina mass fraction increased by approximately 50% about 20 seconds after feeding commenced.
- Other species showed only a small variation in mass fraction both across the cell and with time.
- Reaction rate for the dissolution reaction was found to be reasonably constant throughout the cell.
- The equilibrium reaction rate was high in the ACD under the anode and highest for the part of the anode near the inter-anode gap. In some parts of the side and end channels the equilibrium reaction was predicted to go in the reverse direction.

ACKNOWLEDGMENTS

The present work was supported by the project “Gas and Alumina Distribution and Transport” (GADT), financed by the Research Council of Norway and Hydro Primary Metal Technology. Permission to publish the results is gratefully acknowledged.

The authors wish to acknowledge the valuable discussions and advice provided by Asbjorn Solheim on the electro-chemical reactions, rates and processes in aluminium reductions cells.

REFERENCES

ANSYS Workbench / Fluent 14.5, ANSYS Inc., USA. 2013.

FENG, Y.Q., COOKSEY, M. and SCHWARZ, M.P., (2010a), “CFD Modelling of alumina mixing in aluminium reduction cells”, *Light Metals 2010*, 455-460.

FENG, Y.Q., YANG, W., COOKSEY, M. and SCHWARZ, M.P., (2010b), “Development of Bubble Driven Flow CFD Model Applied for Aluminium Smelting Cells”, J. Comp. Multiphase Flows, 2(3), 179-188.

FENG, Y.Q., COOKSEY, M. and SCHWARZ, M.P., (2011), “CFD Modelling of alumina mixing in aluminium reduction cells”, *Light Metals 2011*, 543-548.

FROLOV, A.V., GUSEV, A.O., ZAIKOV, Y.P., KHRAMOV, A.P., SHUROV, N.I., TKACHEVA, O.Y., APISAROV, A.P. and KOVROV, V.A. (2007), “Modified alumina-cryolite bath with high electrical conductivity and dissolution rate of alumina”, *Light Metals 2007*, 571-576.

GAGNON, F., ZIEGLER, D. and FAFARD, M., (2011), "A preliminary finite element electrochemical model for modelling ionic species transport in the cathode block of a Hall-Héroult cell"**,** *Light Metals*, 537-542.

GUSBERTI, V., SEVERO, D.S., WELCH, B.J., and SKYLLAS-KAZACOS, M., (2012), "Modeling the mass and energy balance of different aluminium smelting cell technologies", *Light Metals 2012*, 929-934.

ISHII, M. and ZUBER, N., (1979), *AIChE J.*, **25**, 843-855.

LOPEZ DE BERTODANO, M., (1991), *Turbulent bubbly flow in a triangular duct*, Ph.D. Thesis, Rensselaer Polytechnic Institute, New York.

KVANDE, H. (1986), "The structure of alumina dissolved in cryolite melts", *Light Metals*, 451-459.

MANDIN, P., WATHRICH, R. and ROUSTAN, H. (2009) "Industrial Aluminium Production: the Hall-Heroult Process Modelling" in *ECS Transactions*, p. 1, Industrial Electrochemistry and Electrochemical Engineering General Session - 215th ECS Meeting, San Francisco, CA.

MOXNES, B., SOLHEIM, A., LIANE, M., SVINSÅS, E. and HALKJELSVIK, A., (2009), *Light Metal*, 461-466.

OLMOS, E., GENTRIC, C. and MIDOUX, N., (2003) "Numerical description of flow regime transitions in bubble column reactors by a multiple gas phase model", Chemical Engineering Science, **58**, 2113-2121.

SMITH, B.L., (1998) "On the modelling of bubble plumes in a liquid pool", *Applied Mathematical Modelling*, **22**, 773-797.

SOLHEIM, A. (2012), "Concentration gradients of individual anion species in the cathode boundary layer of aluminium reduction cells", *Light Metals*, 665-670.

SOLHEIM, A., (2013), Personal Correspondence.

SOLHEIM, A. and STERTEN, A., (1999) "Activity of Alumina in the System NaF-AlF_3-Al_2O_3 at NaF/AlF_3 Molar rations ranging from 1.4 to 3", *Light Metals 1999*, 445-452.

SOLHEIM, A. ROLSETH, S., SKYBAKMOEN, E. STØEN, L. STERTEN Å. and STØRE, T. (1995) "Liquidus Temperature and Alumina Solubility in the System Na_3AlF_6-AlF_3-LiF-CaF_2-MgF_2", Light Metals 1995, 451-460.

WITT, P.J., FENG, Y.Q., EICK, I. and SCHWARZ, M.P., (2012), "Modelling bubble flow with CFX and Fluent for aluminium reductions cells", *9th Int. Conference on CFD in the Mineral and Process Industries*, CSIRO, Melbourne, Australia, 10-12 Dec.